TOXICOLOGICAL SCIENCES **130(2)**, 391–404 (2012)
doi:10.1093/toxsci/kfs241
Advance Access publication August 7, 2012

Neonatal Exposure to the Cyanobacterial Toxin BMAA Induces Changes in Protein Expression and Neurodegeneration in Adult Hippocampus

Oskar Karlsson,*,†,[1] Anna-Lena Berg,‡ Anna-Karin Lindström,‡ Jörg Hanrieder,* Gunnel Arnerup,‡ Erika Roman,* Jonas Bergquist,§ Nils Gunnar Lindquist,* Eva B. Brittebo,* and Malin Andersson*

*Department of Pharmaceutical Biosciences, Uppsala University, 751 24 Uppsala, Sweden; †Department of Environmental Toxicology, Uppsala University, 752 36 Uppsala, Sweden; ‡AstraZeneca R&D Södertälje, Safety Assessment, 151 85 Södertälje, Sweden; and §Department of Physical and Analytical Chemistry, Uppsala University, 751 24 Uppsala, Sweden

[1]To whom correspondence should be addressed. Fax: +46-184714253. E-mail: oskar.karlsson@farmbio.uu.se.

Received March 14, 2012; accepted July 30, 2012

The cyanobacterial toxin β-N-methylamino-L-alanine (BMAA) has been proposed to contribute to neurodegenerative disease. We have previously reported a selective uptake of BMAA in the mouse neonatal hippocampus and that exposure during the neonatal period causes learning and memory impairments in adult rats. The aim of this study was to characterize effects in the brain of 6-month-old rats treated neonatally (postnatal days 9–10) with the glutamatergic BMAA. Protein changes were examined using the novel technique Matrix-Assisted Laser Desorption Ionization (MALDI) imaging mass spectrometry (IMS) for direct imaging of proteins in brain cryosections, and histological changes were examined using immunohistochemistry and histopathology. The results showed long-term changes including a decreased expression of proteins involved in energy metabolism and intracellular signaling in the adult hippocampus at a dose (150 mg/kg) that gave no histopathological lesions in this brain region. Developmental exposure to a higher dose (460 mg/kg) also induced changes in the expression of S100β, histones, calcium- and calmodulin-binding proteins, and guanine nucleotide-binding proteins. At this dose, severe lesions in the adult hippocampus including neuronal degeneration, cell loss, calcium deposits, and astrogliosis were evident. The data demonstrate subtle, sometimes dose-dependent, but permanent effects of a lower neonatal dose of BMAA in the adult hippocampus suggesting that BMAA could potentially disturb many processes during the development. The detection of BMAA in seafood stresses the importance of evaluating the magnitude of human exposure to this neurotoxin.

Key Words: **ALS/PDC; α-synuclein; neuronal calcification; MALDI imaging mass spectrometry; proteomics; hippocampus; CA1.**

Cyanobacteria (blue-green algae) produce several toxins associated with adverse health effects in animals and humans. Recent reports have indicated that most cyanobacteria can produce the neurotoxic nonprotein amino acid β-N-methylamino-L-alanine (BMAA) (Banack *et al*., 2007; Cox *et al*., 2005). Cyanobacteria are ubiquitous microorganisms capable of massive increase in numbers (algal blooming) in various types of waters all over the world, and BMAA has been detected in several water systems including temperate aquatic ecosystems (Caller *et al*., 2009; Esterhuizen and Downing, 2008; Metcalf *et al*., 2008). Recreational water activity is a primary cause of cyanotoxin exposure in addition to contaminated food and drinking water (Freeman, 2010; Valerio *et al*., 2010). The presence of BMAA in molluscs and fish used for human consumption suggests that BMAA may bioaccumulate in aquatic food chains (Brand *et al*., 2010; Jonasson *et al*., 2010).

Dietary exposure to BMAA has been suggested to be involved in the etiology of amyotrophic lateral sclerosis/Parkinsonism-dementia complex (ALS/PDC) on the island of Guam (Banack and Cox, 2003; Spencer *et al*., 1987), but the role of BMAA in neurodegenerative disease remains controversial (Steele and McGeer, 2008). The neurotoxin accumulates in a terrestrial human food chain on the island and is reported to be present in brain tissue of ALS/PDC patients (Banack and Cox, 2003; Murch *et al*., 2004). BMAA has also been reported to be present in brains of Alzheimer's disease patients and ALS patients (Murch *et al*., 2004; Pablo *et al*., 2009), but so far the analytical data are conflicting (Montine *et al*., 2005; Snyder *et al*., 2009). In addition, an association between cyanobacterial blooms in New Hampshire and development of ALS has recently been suggested (Caller *et al*., 2009).

Our previous autoradiographic studies revealed that ^{3}H-BMAA-derived radioactivity was transferred across the blood-brain barrier in neonatal mice, with a preferential uptake in the hippocampus and the striatum (Karlsson *et al*., 2009b). In contrast, the transfer of BMAA to the adult rodent brain was less pronounced and no regio-selective localization was observed (Karlsson *et al*., 2009a; Smith *et al*., 1992). The mixed glutamate receptor agonist BMAA is considered to have a low neurotoxic potency in adult rodents (Karamyan and Speth, 2008; Perry *et al*., 1989). We have recently reported, however, that exposure to BMAA during the neonatal period (postnatal days [PND] 9–10)

caused spatial learning and memory impairments in adulthood (Karlsson *et al*., 2009c, 2011). The neonatal period is a critical phase of brain development, and disturbances of the developmental processes can manifest as permanent changes in adults (Eriksson, 1997; Eriksson *et al*., 2000). In order to understand the mechanisms of BMAA-induced neurobehavioral alterations, more studies on the effects of BMAA in the hippocampus are needed, as this brain area is essential for learning and memory.

In this study, we applied Matrix-Assisted Laser Desorption Ionization (MALDI) imaging mass spectrometry (IMS) to search for BMAA-induced protein changes in various brain regions of adult rats following neonatal exposure to BMAA. MALDI IMS has the capability to analyze several proteins simultaneously and the key strength compared with non-IMS methods is the ability to give direct spatial localization together with quantitative estimates of the analytes (Caprioli *et al*., 1997). In a second part of the study, we used available cryosections from the MALDI IMS study to characterize histological changes in the hippocampus. The results show that BMAA induced long-term changes including decreased expression of proteins involved in energy metabolism and intracellular signaling in the adult hippocampus at a dose (150 mg/kg) that gave no histopathological lesions in this brain region. Developmental exposure to a higher dose (460 mg/kg) induced changes in the expression of S100β, histones, calcium- and calmodulin-binding proteins as well as guanine nucleotide-binding proteins. At this dose, severe lesions in the adult hippocampus including neuronal degeneration, cell loss, calcium deposits, and astrogliosis were evident.

MATERIALS AND METHODS

Chemicals

L-BMAA hydrochloride (≥ 97%) was obtained from Sigma-Aldrich Co. (St Louis, MO). Unless otherwise stated, all chemicals were obtained from Sigma-Aldrich Co.

Experimental Design

The experimental design and the BMAA doses examined were identical to those previously reported to induce cell death in the hippocampus in neonates and cognitive changes in adult animals (Karlsson *et al*., 2009c, 2011). Pregnant outbred Wistar rats were obtained from Scanbur BK AB (Sollentuna, Sweden). The dams were housed alone in a standard macrolon cage containing woodchip bedding and nesting material. The animals were maintained on standard pellet food (R36 Labfor; Lantmännen, Kimstad, Sweden) and water *ad libitum*, and were housed in a temperature- and humidity-controlled environment on a 12-h light/dark cycle. The litters were cross-fostered at the day of birth, PND 0. Each new litter contained eight pups, with an equal distribution of males and females as far as possible. The male pups were given one daily sc injection (20 µl/g) of BMAA 150 mg/kg (corresponding to 200 mg/kg BMAA HCl; $n = 8$) or 460 mg/kg (corresponding to 600 mg/kg BMAA HCl; $n = 7$) freshly dissolved in Hanks' balanced salt solution, or vehicle ($n = 7$), for 2 days on PND 9–10. The short- and long-term behavioral effects of BMAA in these animals have been published separately (Karlsson *et al*., 2009b,c). After weaning on PND 22 and onwards, two to four male rats were housed together in standard macrolon cages (59 × 38 × 20 cm) in their respective treatment groups. All animal experiments were approved by the Uppsala Ethical Committee on Animal Experiments and followed the guidelines of Swedish legislation on animal experimentation (Animal Welfare Act SFS1998:56) and European Union legislation (Convention ETS123 and Directive 86/609/EEC).

Histopathology and Immunohistochemistry

The animals were killed by decapitation at 23 weeks of age, the brains were quickly frozen in dry ice and stored at −80°C. Coronal cryosections from the right hemisphere of the brain were used for histopathology and immunohistochemistry (IHC). Brain sections from all animals were stained with hematoxylin and eosin (H&E) and examined by light microscopy. Selected sections were stained with Congo Red, for identification of amyloid, and with von Kossa's stain, for detection of calcium. A neuropathologist conducted the morphological examination and histopathological scoring.

IHC was performed on brain sections from animals with morphological changes (460 mg/kg), using antibodies against glial fibrillar acidic protein (GFAP), neurofilament, amyloid-β (Aβ), tau protein, α-synuclein, and ubiquitin. Cryosections for GFAP, α-synuclein, and neurofilament staining were fixed in 2% phosphate-buffered paraformaldehyde for 10 min at + 4°C prior to staining. Cryosections for the other markers were fixed in 50% cold (+ 4°C) acetone for 30 s followed by 100% cold (+ 4°C) acetone for 3 min before being air-dried and stained. IHC for GFAP, neurofilament, Aβ, tau/AT8, α-synuclein, and ubiquitin was performed on the staining module Discovery XT. Ventana Medical Systems Inc. (Tucson, AZ), supplied all solutions for pretreatment, antibody dilution, detection, counterstaining, and rinsing steps. IHC for detection of tau protein using the Invitrogen antibody (AHB0042) was performed on the staining module IntelliPATH FLX. Biocare Medical (Concord, CA) supplied all solutions for antibody dilution, detection, counterstaining, and rinsing steps. Details of primary and secondary antibodies, and detection systems used, are given in Supplementary table 1. Slides stained without primary antibody (only antibody diluent in the primary antibody step) served as negative controls.

MALDI IMS

Coronal cryosections were obtained from the right hemisphere of all animals at the level of hippocampus (−3.36 mm relative to the bregma; Paxinos and Watson, 2007). The brain sections (12 µm) were thaw-mounted on conductive glass slides suitable for MALDI IMS analysis (Bruker Daltonics, Bremen, Germany). The sections were dried under vacuum and stored at −20°C. In total brain sections from 20 animals were analyzed (vehicle control; $n = 6$, 150 mg/kg BMAA; $n = 8$; 460 mg/kg BMAA; $n = 6$). Due to technical error in the processing of the glass slides, two animals, one control and one high-dose animal, could not be analyzed.

In order to fix tissue and remove excessive salts, the cryosections were washed in 70% (30 s) and 95% ethanol (2 × 30 s) as previously described (Andersson *et al*., 2008). The sections were dried face up in a vacuum desiccator. For assessment of proteins, the MALDI matrix (10 mg/ml sinapinic acid, 5 mg/ml 2´,4´,-dihydroxyacetophenone [DHAP] in 60% ethanol, 10% ammonium acetate and 0.3% trifluoroacetic acid) was applied using a chemical inkjet printer (CHIP-1000, Shimadzu, Japan). Droplets of 100 pl were placed in arrays (15 drops per pass for 24 passes) over the sections at a spatial resolution of 300 × 300 µm. Mass spectra were acquired using an Ultraflex II (Bruker Daltonics), equipped with smart beam technology, operating in linear positive mode.

Prior to image analysis, each MALDI plate was externally calibrated using a standard protein mix (Protein Calibration Standard I, *m/z* range 3–25 kDa, Bruker Daltonics). A mass range of 3.5–22.3 kDa was analyzed with a laser frequency of 100 Hz. Data sequence preparation, MS acquisition and visualization was performed using the FlexImaging and FlexControl software (v 3.0, Bruker Daltonics).

Data postprocessing by means of baseline reduction, normalization by total ion current (TIC), and data reduction was performed as previously described (Hanrieder *et al*., 2011, 2012; Ljungdahl *et al*., 2011). The TIC before normalization was compared and displayed the characteristic normal distribution within each group and was not statistically different between the groups, thus minimizing the risk of introducing artificial errors. A peak was only included if it was present in at least 10% of all spectra, corresponding to about 250 out of a total 2500 spectra for CA1 and 400 for DG. In total, the peak limits were calculated for 1061 peaks for

CA1 and 1043 peaks in DG, and peak area integration within the corresponding limits was performed with a self-written R script (Hanrieder *et al*., 2012).

A nonparametric Kruskal-Wallis test followed by the Mann-Whitney's *U*-test was used for intergroup comparisons of single proteins. Differences were considered statistically significant at $p < 0.05$.

Protein Identification

In solution digestion followed by nanoliquid chromatography-electrospray ionization/multistage MS. Forty brain sections (20 µm) from a nontreated control rat were collected in a 1.5-ml sample vial (LoBind, Eppendorf, Hamburg, Germany). A volume of 0.5 ml 50% Acetonitrile (ACN) and 0.2% trifluoracetic acid was added, and the tissue was homogenized manually with a micropestle twice. For protein precipitation, six volumes of ice-cold acetone were added to the supernatant and the sample was stored at −20°C overnight. The precipitated protein fraction was reconstituted in 1 ml 1% HAc and high-mass proteins removed by a 30-kDa mass weight cutoff filter (MWCO 30, Millipore). The flow through was then fractionated using C8 reversed phase high-performance liquid chromatography (HPLC; 4.6 mm × 150 cm, 5 µm particle size, 300 Å pore size, Kromasil, Akzo Nobel, Gothenburg, Sweden), and the intact protein masses were analyzed by MALDI MS as previously described (Aerni *et al*., 2006; Andersson *et al*., 2008; Groseclose *et al*., 2007). Fractions containing target proteins were reduced, alkylated, and digested by trypsin for liquid chromatography-multistage MS (LC-MS/MS) analysis (Proteomics Core Facility, Gothenburg University, Sweden). Mascot (v. 2.2, Matrix Science) MS/MS search uses the following specifications: species (rat); fixed modifications (carbamidomethyl); variable modifications (oxidation M); mass tolerance-MS (10 ppm) and mass tolerance-MSMS (0.8 Da); enzyme (trypsin), missed cleavages (1), and charge states (1+, 2+, and 3+).

For visualization of the distribution of specific tryptic peptides, on tissue trypsin digestion of one hippocampal section from a high-dosed animal with a hippocampal lesion (460 mg/kg) was performed as previously described (Andersson *et al*., 2008; Groseclose *et al*., 2007). The digested section was analyzed as above using an Ultraflex II operated with positive polarity in reflector mode and spectra acquired in the range of *m/z* 500–6000. Two nondigested adjacent sections were spotted with DHAP/SA for imaging of intact proteins.

Immunofluorescence Verification of MALDI IMS Results

Double-antigen fluorescent IHC was performed on brain sections from selected animals using rabbit anti-histone H4, rabbit anti-histone H3 (1:100, Upstate, Lake Placid, NY), or rabbit anti-S100β (1:200, Abcam, Cambridge) in combination with mouse anti-GFAP (1:500, Millipore, Temecula, CA) as primary antibodies. Rabbit anti-neurogranin (1:100, Abcam) in combination with mouse anti-NeuN (1:100, Millipore) were also used as primary antibodies. The fluorescent secondary antibodies anti-rabbit-Alexa Fluor 488 (1:200, Invitrogen, Carlsbad, CA) and anti-mouse-Alexa Fluor 555 (1:200, Invitrogen) were used for visualization. Cell nuclei were stained by 4,6-diamidino-2-phenylindole (DAPI). Sections incubated without primary antibody (only the antibody diluent, 2.5% horse serum in phosphate-buffered saline, in the primary antibody step) served as negative controls.

RESULTS

Effects of BMAA on Hippocampus, Striatum, and Substantia Nigra Histology

The histopathological findings in cryosections that were available from the MALDI IMS study are summarized in Table 1 and representative images are shown in Figure 1A–M.

Vehicle control. There was a normal appearance and cellularity in the hippocampus (Fig. 1A), striatum, and substantia nigra. In the hippocampus, there was also a normal GFAP immunoreactivity (Fig. 1D) but no specific immunostaining against neurofilament (Fig. 1M), phosphorylated tau, or synuclein (Fig. 1K). In addition, there was no, or very faint, staining for ubiquitin of CA1 neurons and astrocytes (Fig. 1L). No histochemical staining for calcium and amyloid was observed in the controls.

TABLE 1
Histopathological Lesions[a] in the Adult Brain of Rats Treated With BMAA on PND 9–10

Treatment	Animal No.	Hippocampus CA1 regionScoring of alterations observed
BMAA 460 mg/kg	9, 13, 14	No major changes
	10	+Neuronal degeneration/necrosis +Deposition of birefringent material
	11	++++Neuronal degeneration/necrosis ++++Deposition of birefringent material ++++Astrogliosis
	12, 18	++++Neuronal degeneration/necrosis +++Deposition of birefringent material +++Astrogliosis
BMAA 150 mg/kg	20–27	No changes
Vehicle	2–8	Normal histology/IHC

Notes. The brains were studied at the level of striatum, hippocampus/thalamus, and substantia nigra.

Scoring system: -, none; +, minimal/occasional cells; ++, slight/scattered cells; +++, moderate/moderate number of cells; and ++++, marked/numerous cells.

Other brain regions (e.g., striatum, cingulate cortex, dentate gyrus, retrosplenial granular cortex, and substantia nigra) did not show any histopathological lesions.

[a]The histopathological examination was based on morphology (H&E staining) and GFAP IHC.

BMAA 150 mg/kg. The general morphology of the hippocampus, striatum, and substantia nigra did not differ from that of the control rats (Fig. 1B). There was no increased GFAP staining in these brain regions compared with the controls (Fig. 1E). No other immunohistochemical stainings were performed.

BMAA 460 mg/kg. Four out of seven rats showed distinct histopathological lesions in the CA1 segment of the hippocampus. In these rats, there was minimal to marked neuronal loss, accompanied by astrogliosis, as evidenced by prominent GFAP staining in the CA1 region (Fig. 1F). Remaining neurons were degenerating or necrotic, and several contained a granular, faintly greenish, birefringent material (Fig. 1C). Some of this material seemed to be located extracellularly, although this was difficult to assess due to the presence of cryo-related artifacts. von Kossa staining revealed a strong and distinct staining of the birefringent structures in the hippocampus, demonstrating the presence of calcium deposits (Fig. 1M). Staining with Congo Red for identification of amyloid was negative and did not differ from vehicle controls (data not shown). There was a moderately increased staining intensity for α-synuclein compared with controls (Fig. 1H)

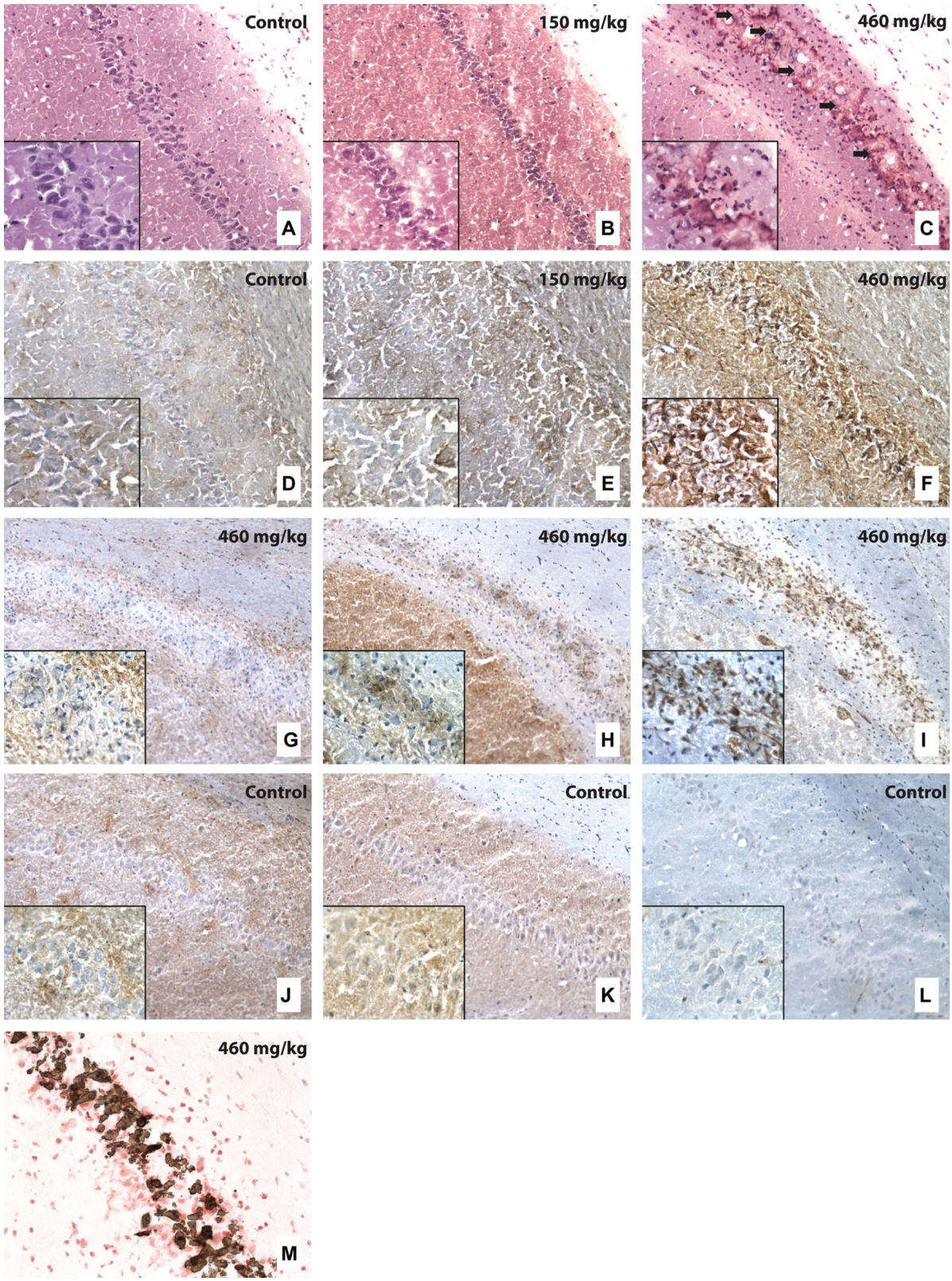

FIG. 1. Histological studies on hippocampal sections of adult rats neonatally treated on PND 9–10 with BMAA or vehicle.

Upper panel (A–F): H&E staining (A–C) and IHC (D–F) showing the expression of GFAP for detection of reactive astrocytes in the hippocampus (CA1 segment) of rats treated neonatally on PND 9–10 with BMAA or vehicle. The vehicle-treated control rat shows normal cellularity of the CA1 segment of hippocampus (A) and normal GFAP immunoreactivity in the same area (D). The rat treated with 150 mg/kg BMAA (B and E) does not differ from the control rat (A and D). The rat treated with 460 mg/kg BMAA (C) displays marked neuronal cell loss in the CA1 segment, as well as deposition of a birefringent granular material (arrows) both intra-and extracellularly.

and a strong positive staining for ubiquitin in the CA1 region of the hippocampus (Fig. 1I). Astrocytes were positively stained for ubiquitin, as were some of the degenerating and/or calcified neurons although not as intensely as the astrocytes. The immunohistochemical staining for neurofilament or phosphorylated tau did not differ from the nonexposed controls (Fig. 1G). Other segments of the hippocampus, including the DG, appeared histologically normal.

No obvious histopathological changes, nor increased astrogliosis, were observed in other brain regions such as cingulate cortex, retrosplenial granular cortex, striatum, or substantia nigra (data not shown).

Effects of BMAA on Protein Expression Determined by MALDI IMS

A novel MALDI matrix mix consisting of part sinapinic acid and part DHAP dissolved in 60% ethanol was evaluated and the resulting rat brain spectra were identical to those obtained using earlier published protocols (Fig. 2B; Aerni *et al*., 2006; Andersson *et al*., 2008). For statistical analysis of BMAA-induced changes of peak intensities, several regions of interest (ROI) in the cryosections had to be defined and therefore the scanned tissue sections were stained with toluidine blue after MS acquisition (Fig. 2A). A picture of the stained sections was then co-registered with the corresponding scan of the spotted section. Histology as well as ion distribution maps of several proteins were used to first define the entire hippocampus area.

Effects of BMAA on Protein Expression in the Hippocampus

Low variance (15% relative standard deviation) was observed for all peaks detected in the hippocampal ROI within each treatment group and 34 peaks displayed BMAA-induced alterations in protein ion intensities versus vehicle control. Visualization of several peaks revealed that most up- or down-regulated proteins were confined to the CA1 in animals of the high-dose group, indicating that CA1 was the most affected region in BMAA-treated animals.

Regional analysis of BMAA-induced changes revealed 41 and 18 significantly changed protein peaks in the CA1 and the DG region of both high- and low-dose groups versus control, respectively. Three of the animals (Nos 11, 12, and 18) in the high-dose group differed markedly from the vehicle controls and showed the largest number of BMAA-induced changes in peak intensities (154 peaks in CA1 and 102 in DG, $p < 0.05$ vs. vehicle controls or low-dose BMAA). Indeed, these were the animals displaying severe hippocampal lesions of the CA1, as described above. Among these animals, several proteins involved in transmembrane signaling in neurons displayed a 2-fold reduced peak intensity, including neurogranin, guanine nucleotide-binding protein gamma-7 subunit (Gng7) and Gng2 (Fig. 3; $p < 0.05$ vs. vehicle control and low-dose BMAA).

Calmodulin and the calmodulin-binding protein BASP1/NAP22A also displayed a similar reduction of the peak intensities in the CA1 of high-dose animals (0.65- and 0.40-fold change, $p < 0.05$ vs. vehicle control and low-dose BMAA). A reduction of the ubiquitin peak intensities was detected, but overall group comparisons did not reach statistical significance (Fig. 3; $p = 0.076$ high-dose group vs. vehicle controls).

Several cytochrome c oxidase polypeptides (VIIa, VIc-2, VIII, Via, and cytochrome b-c1 complex subunit 8) of the mitochondrial electron transport chain also displayed about a 2-fold reduction of levels in CA1 ($p < 0.05$ vs. vehicle controls). The cytochrome c oxidase polypeptides in the low-dose group showed reduced levels of these proteins in CA1 but were not statistically significant compared with controls. However, the analysis of cytochrome c oxidase in the DG revealed a significant reduction of protein peak intensities in both the 150 and 460 mg/kg BMAA-treatment groups compared with the vehicle control ($p < 0.05$ vs. vehicle control, 23 and 42% decrease, respectively).

Significantly increased levels of histones were detected in CA1 of the three most affected animals (460 mg/kg), including histone H2, histone H3, and histone H4 (55–100% increase; Fig. 4). Most proteins (94 out of 154) were significantly increased in CA1 of these animals, for example, two unidentified proteins with a mass of 10.6 and 11.7 kDa (200 and 250% increase, respectively; Fig. 5). Interestingly, secretoneurin (*m/z* 3652.98) displayed elevated levels in the DG of high-dose animals (1.38-fold change vs. control; $p < 0.05$). The chromo- and secretogranins are known modulators of inflammatory processes, although much is still unknown about their molecular function in the CNS (Helle, 2010).

Other proteins with unknown identity were significantly decreased both in CA1 and DG, for example, an ion with a mass of 5636 Da that was significantly decreased in all BMAA-treated animals. By contrast, the peak at *m/z* 7242 Da represents

←

Strong GFAP immunoreactivity (F), consistent with pronounced astrogliosis, is present in the same region as shown in (C). The insets show details of the CA1 segment. Magnifications: A–F lens ×10; inset in left corner of the images lens ×40.

Middle panel (G–L): IHC showing the staining for neurofilament (J and M), α-synuclein (K and N), and ubiquitin (L and O) in the CA1 segment of rats treated neonatally on PND 9–10 with 460 mg/kg BMAA or vehicle. The expression of neurofilament does not differ between a rat treated with BMAA (J) and a vehicle control rat (M). There is a moderately increased expression of α-synuclein in the BMAA-treated rat (K) compared with the control rat (N). Ubiquitin is strongly stained within the CA1 region in the BMAA-treated rat (L), compared with the control rat (O), which shows only faint staining. The insets show details of the CA1 segment. Magnifications: J–O lens ×10; inset in left corner of the images lens ×40.

Lower panel (M): von Kossa's stain demonstrates that the birefringent material observed in the H&E-stained sections consists of calcium deposits (brown). Magnification: lens ×20.

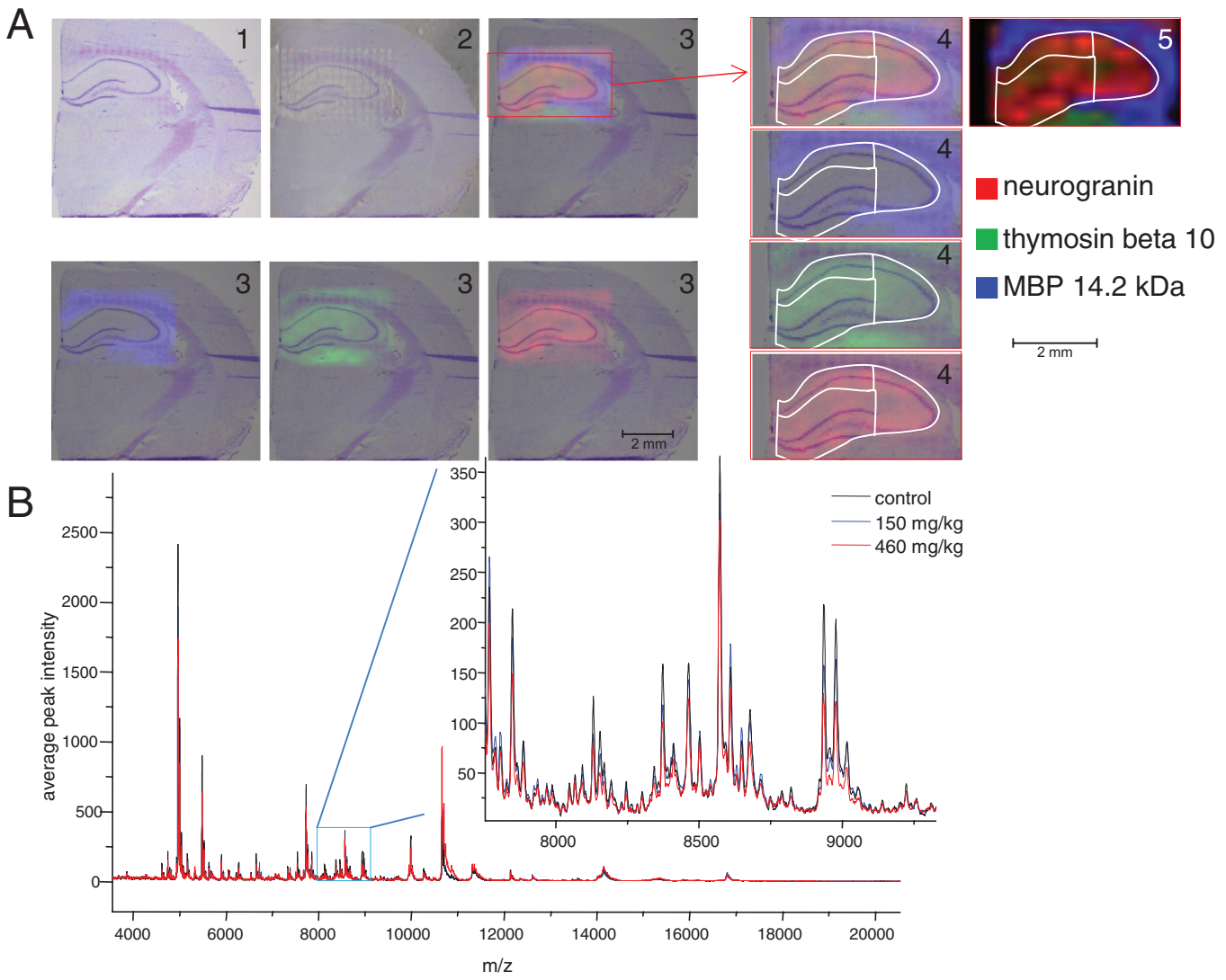

FIG. 2. MALDI IMS of hippocampal sections of adult rats neonatally treated on PND 9–10 with vehicle. (A) Distinct ROI were determined for the entire hippocampus, CA1 and DG of each brain section using both histology and MALDI IMS ion maps. (1) The photomicrograph of the toluidine blue-stained section was co-registered with (2) the image of the spotted section used for MALDI IMS acquisition, here shown at 50% translucency. (3) Multiplexing translucent ion distribution maps of myelin basic protein (MBP) (blue), thymosin β-10 (green), and neurogranin (red) revealed distinct topographical distributions. (4) A composite MALDI IMS shown at 50% translucency and (5) 0% translucency of all three ions at higher magnification demonstrate how the hippocampus was defined dorsally and laterally by white matter fiber tracts (MBP), and ventrally by high thymosin β-10 intensity in the lateral posterior thalamic nucleus. The CA1 ROI only included the medial part of CA1 as defined by the lateral limit of the DG ROI. (B) Average hippocampal mass spectrum from BMAA- and vehicle-treated rats. Over 1000 peaks in the mass range of 3.5–20 kDa were detected and analyzed by MALDI IMS. Most ion intensities displayed a high degree of overlap between the treatment groups, demonstrating good IMS reproducibility (insert).

a peak that was increased in the DG in both treatment groups (Fig. 5). In addition, several unknown protein peaks were dose-dependently up (9) or down (2; DG only) regulated in CA1 (2 peaks) and DG (9 peaks) ($p < 0.05$ high dose vs. control and low dose; $p < 0.05$ low dose vs. vehicle).

Protein Identification and Validation by On-tissue Digestion Combined With MALDI IMS

Protein peaks were identified by HPLC separation followed by trypsinization and LC-MS/MS analysis as well as by comparison by mass and tissue distribution previously studied by MALDI IMS (Andersson *et al.*, 2008; Hanrieder *et al.*, 2011; Mathur *et al.*, 2009; Pierson *et al.*, 2004; Skold *et al.*, 2006). Many known protein identities were verified (myelin basic protein; neurogranin; calmodulin; ubiquitin, histones H2, H3.1, and H4; and cytochrome c oxidase polypeptides VIIa, VIa) and some previously unknown peaks were identified (cytochrome b-c1 complex subunit 8, *m/z* 9729; cytochrome c oxidase polypeptides VIc-2 and VIII, *m/z* 8324 and 9719; BASP1, *m/z* 21901; USMG5, *m/z* 6277.4; secretoneurin *m/z* 3652.98).

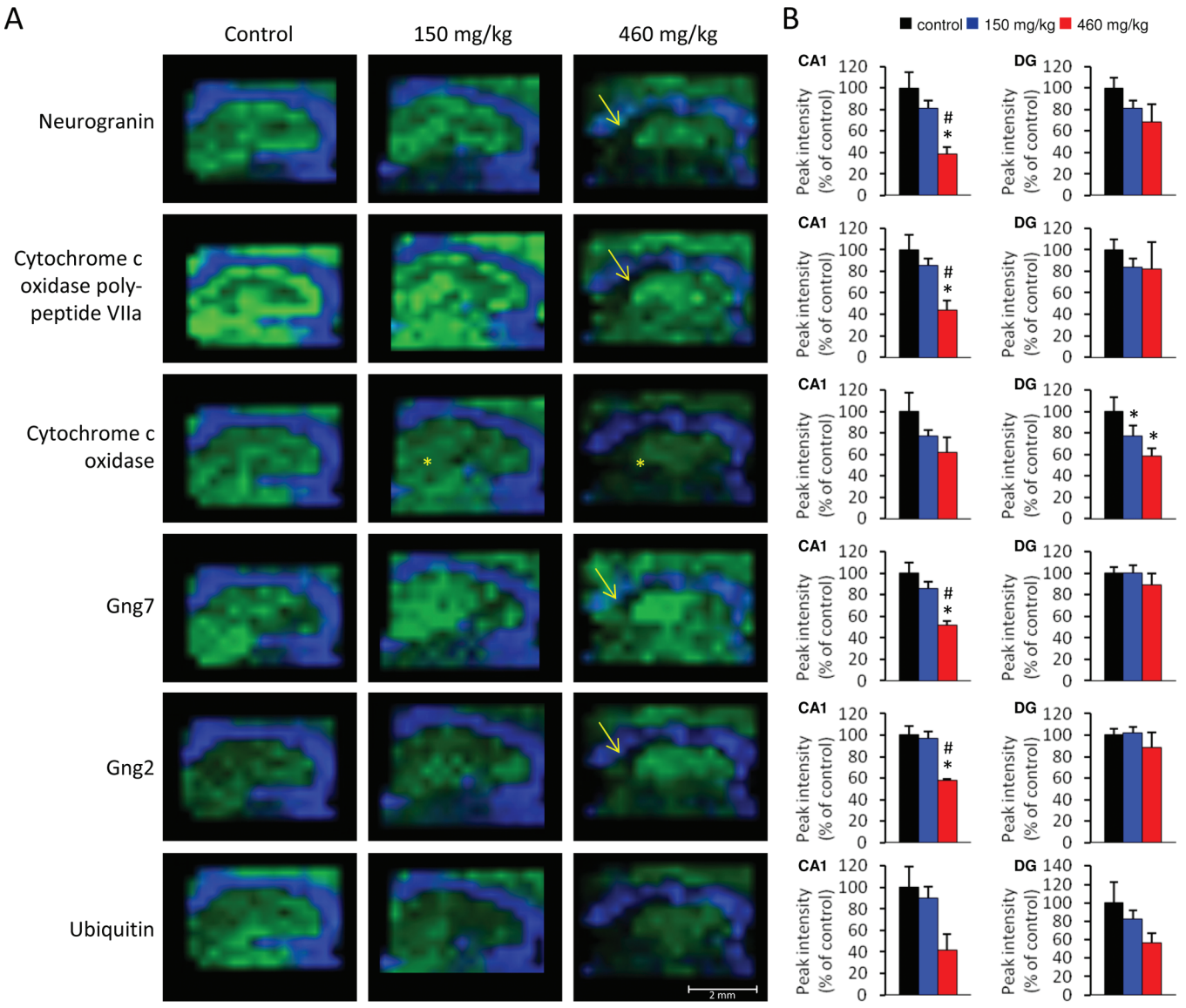

FIG. 3. MALDI imaging of reduced peak intensities in the hippocampus of adult rats neonatally treated on PND 9–10 with BMAA or vehicle. (A) Six selected proteins are shown: neurogranin, cytochrome c oxidase polypeptide VIIa, cytochrome c oxidase, Gng7, Gng2, and ubiquitin. The regional location of reduced protein expression is indicated by arrows in CA1 and by stars in DG of hippocampus. Proteins of interest are highlighted in green and MBP 14.2 kDa (blue) is used to accentuate the dorsal and lateral borders of hippocampus. All proteins were visualized at a fixed absolute intensity threshold. (B) The diagrams show the peak intensity (% of control ± SEM) for the selected proteins in CA1 and DG of hippocampus. Vehicle (black), BMAA 150 mg/kg (blue), and BMAA 460 mg/kg (red). *$p < 0.05$ compared with vehicle control animals and #$p < 0.05$ compared with 150 mg/kg (Kruskal-Wallis test and Mann-Whitney's *U*-test).

For some proteins, including neurogranin, the identities were further validated by visualization of the distribution of tryptic peptides using on-tissue digestion combined with MALDI IMS (Fig. 6). The results also revealed unknown tryptic fragments (*m/z* 4826.67 Da), which were specific for the area with the birefringent material (Fig. 6). In addition, a mass-matching search indicated that the identity of a 10.6-kDa peak could be S100β as the theoretical mass is 10,654 Da and the observed *m/z* was 10,654 Da. Indeed, immunofluorescence analysis showed a distinct increase of S100β immunoreactivity in the CA1 region in a BMAA-treated animal compared with the control (Fig. 7). In the control animal, double-antigen IHC demonstrated that S100β was colocalized with GFAP in the cytoplasm of astrocytes (Fig. 7B). Similarly, many astrocytes in the CA1 region of the high dose-treated animal were double-labeled for S100β and GFAP (Figs. 7E and E').

Immunohistochemical Verification of MALDI IMS Results

In order to verify the cellular localization of changes detected by MALDI IMS, double-antigen IHC was performed on sections from one of the high BMAA dose–treated animals (No. 18) and one vehicle-control animal (No. 7). A distinct loss of

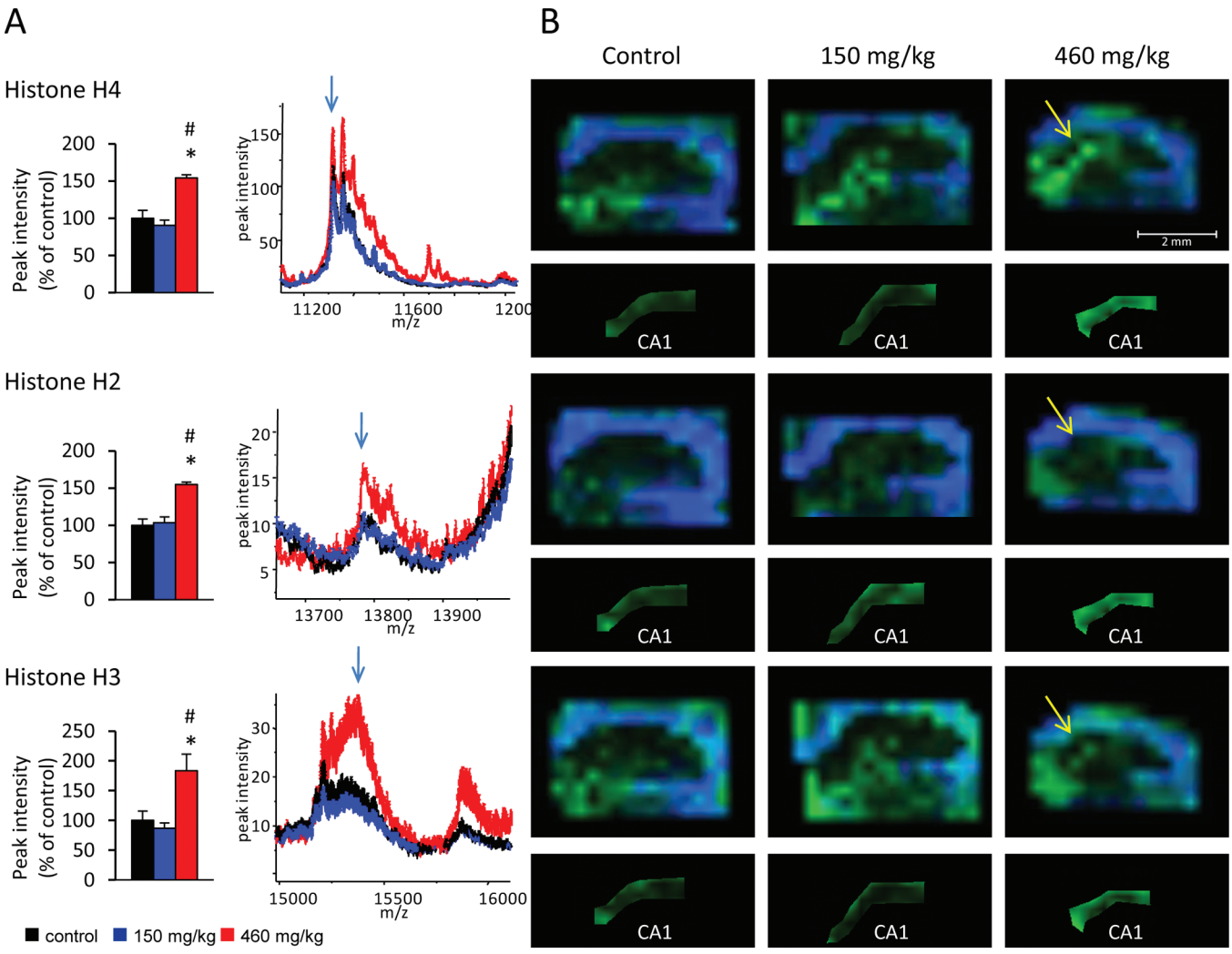

FIG. 4. MALDI ion distribution maps of BMAA-induced up-regulation of histone peak intensities in the CA1 segment of the hippocampus. (A) The diagrams show the peak intensity (% of control ± SEM) for histones H4, H2, and H3 in hippocampus CA1. The corresponding average spectra (± SEM bars) show the protein of interest (arrows) as well as several possible post-translational modifications. Vehicle (black), BMAA 150 mg/kg (blue), and BMAA 460 mg/kg (red). (B) Three of the animals in the high BMAA-treatment group expressed significantly higher levels of all detected histones in the CA1 (arrows) of hippocampus compared with vehicle controls. The small insertions show only CA1 with the protein of interest displayed at higher color intensity. The data analysis also revealed that many post-translational modifications including possible acetylations (+ 42 Da) and phosphorylations (+ 80 Da) were significantly higher in animals with CA1 lesions. Proteins of interest are displayed in green. MBP 14.2 kDa (blue) was used to accentuate the borders of hippocampus. All proteins were highlighted at a fixed absolute intensity threshold. *$p < 0.05$ compared with vehicle control animals and #$p < 0.05$ compared with 150 mg/kg (Kruskal-Wallis test and Mann-Whitney's *U*-test).

neurogranin immunoreactivity in the CA1 region of BMAA-treated animals was accompanied with a dramatic loss of neurons as reflected by the loss of neuronal nuclear antigen NeuN immunopositive nuclei (Figs. 8B and D). The general nuclear staining DAPI revealed an elevation of the number of non-neuronal, NeuN immunonegative cells, which could later be identified as astrocytes using the GFAP antibody (Figs. 8E and F).

The MALDI IMS data revealed an elevation of several histone proteins, including histone H3.1 and histone H4 in high dose BMAA–treated rats. Both H3.1 and H4 antibodies displayed identical findings with a loss of neuronal immunoreactivity and an increase in immunopositive non-neuronal cells, including GFAP-positive astrocytes in the BMAA-treated animal, indicating that the increased number of astrocytes accounts for the increase in histone levels.

DISCUSSION

This study demonstrated that BMAA-elicited selective changes in protein levels in the hippocampus as well as dose-dependent neurodegenerative changes, neuronal cell death, calcification, and astrogliosis in this brain region of rats 6 months after neonatal exposure on PND 9–10. As demonstrated here, MALDI IMS is a powerful technique for neurotoxicological

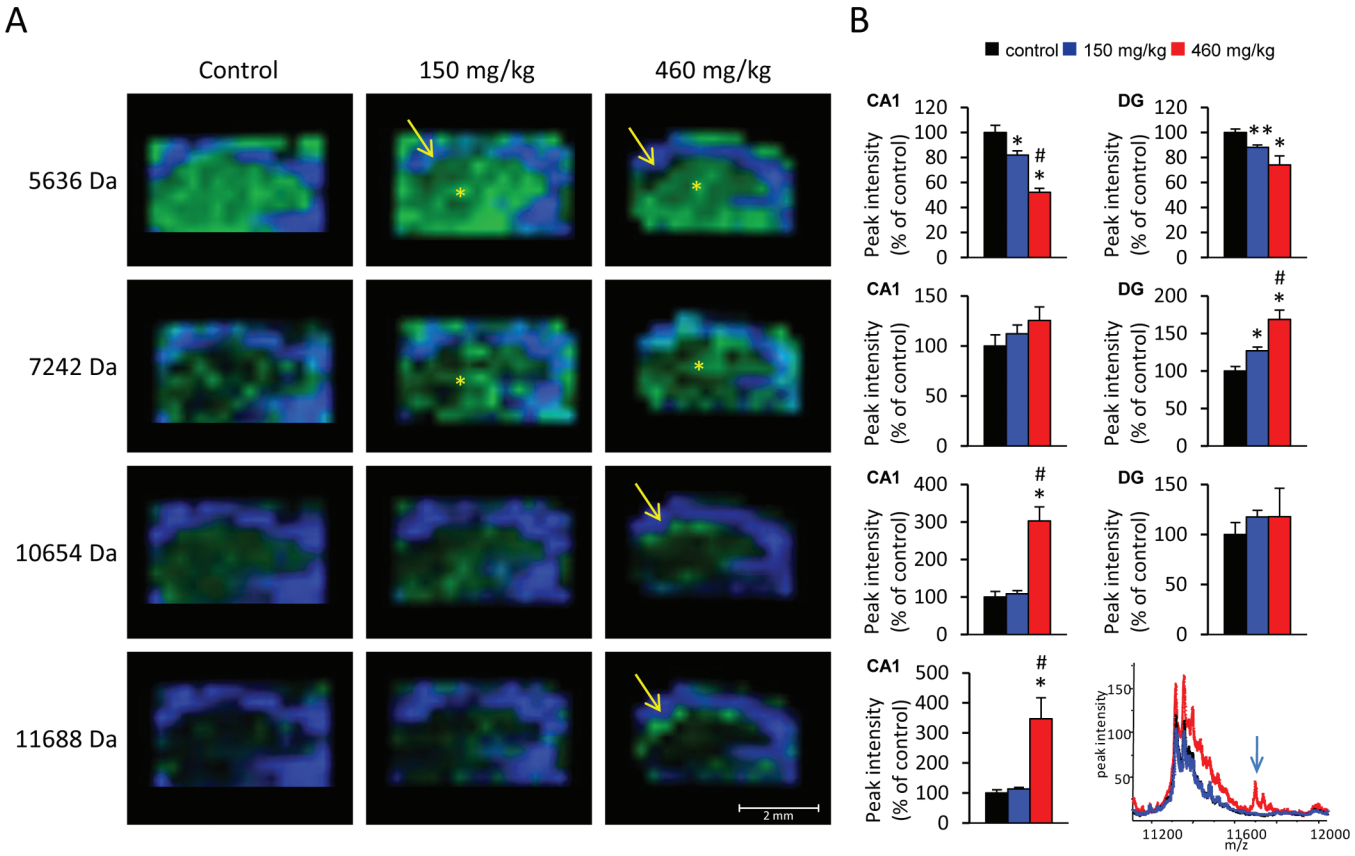

FIG. 5. The MALDI IMS analysis reveals dose-dependent changes in unknown protein levels in the CA1 and DG of adult rats neonatally treated on PND 9–10 with BMAA or vehicle. (A) Examples of protein peaks with unsolved identities that had treatment-related changes of expression in both treatment groups. The ion 5636 Da was significantly decreased in both treatment groups in CA1 (arrows) and DG (stars) of hippocampus, and 7242 Da is an example of an ion that is increased in DG in both treatment groups. The two ions 10,654 and 11,688 Da are examples of protein peaks which were highly increased in CA1 in the three most affected high-dose animals. Proteins of interest were highlighted in green, and MBP 14.2 kDa (blue) was used to highlight borders of the hippocampus. All proteins were visualized at a fixed absolute intensity threshold. (B) The diagrams show the peak intensity (% of control ± SEM) for the unidentified masses in hippocampus CA1 and DG. The average spectra (± SEM) from CA1 show that the 11,688 Da ion (arrow) as well as several possible post-translational modifications are almost exclusively present in the high-dose group. Vehicle (black), BMAA 150 mg/kg (blue), and BMAA 460 mg/kg (red). $*p < 0.05$, $**p < 0.01$ compared with vehicle control animals, and $\#p < 0.05$ compared with 150 mg/kg (Kruskal-Wallis test and Mann-Whitney's *U*-test).

research. The "on tissue"-protein analysis using MALDI IMS did not only uncover animals with neuronal lesions/astrogliosis but also pinpointed CA1 as the most severely affected region in the hippocampus. Animals displaying the most severe histopathological changes also showed the largest number of peak intensity changes and several unknown proteins displayed dose-dependent changes in BMAA-treated animals. In addition, among the known proteins that displayed reduced levels in the high-dose (460 mg/kg) groups, there was a clear tendency toward lower levels also in the low-dose group (150 mg/kg; Fig. 3). For example, the MALDI IMS data showed that the lowest dose (150 mg/kg) induced a decreased level of proteins involved in energy metabolism such as cytochrome c oxidase and its subunit cytochrome c oxidase polypeptide VIIa in the CA1 and the DG of hippocampus, whereas no histopathological lesions were observed in these brain regions. Cytochrome c oxidase is an essential component of the respiratory chain and this enzyme activity is considered as a marker of normal neuronal activity (Wong-Riley, 1989), suggesting that BMAA can induce long-lasting changes in the signaling activity in the adult brain. Indeed, we have reported that this dose level causes impairments in learning and memory in adult rats exposed to BMAA neonatally without any distinct acute morphological changes in the neonatal hippocampus (Karlsson *et al.*, 2009c, 2011). Learning and memory are dependent on the hippocampal function, supporting that neonatal exposure to BMAA may induce a permanently reduced neuronal signaling activity in this brain region.

We have previously reported that neonatal exposure to a higher dose of BMAA (460 mg/kg) induces apoptosis in the DG and CA1 segments of the neonatal hippocampus 24 h after dosing (Karlsson *et al.*, 2011). As shown in this study, this dose also gave rise to distinct histopathological changes including neuronal degeneration, neuronal cell loss, calcium deposits, and astrogliosis in the CA1 segment of the adult

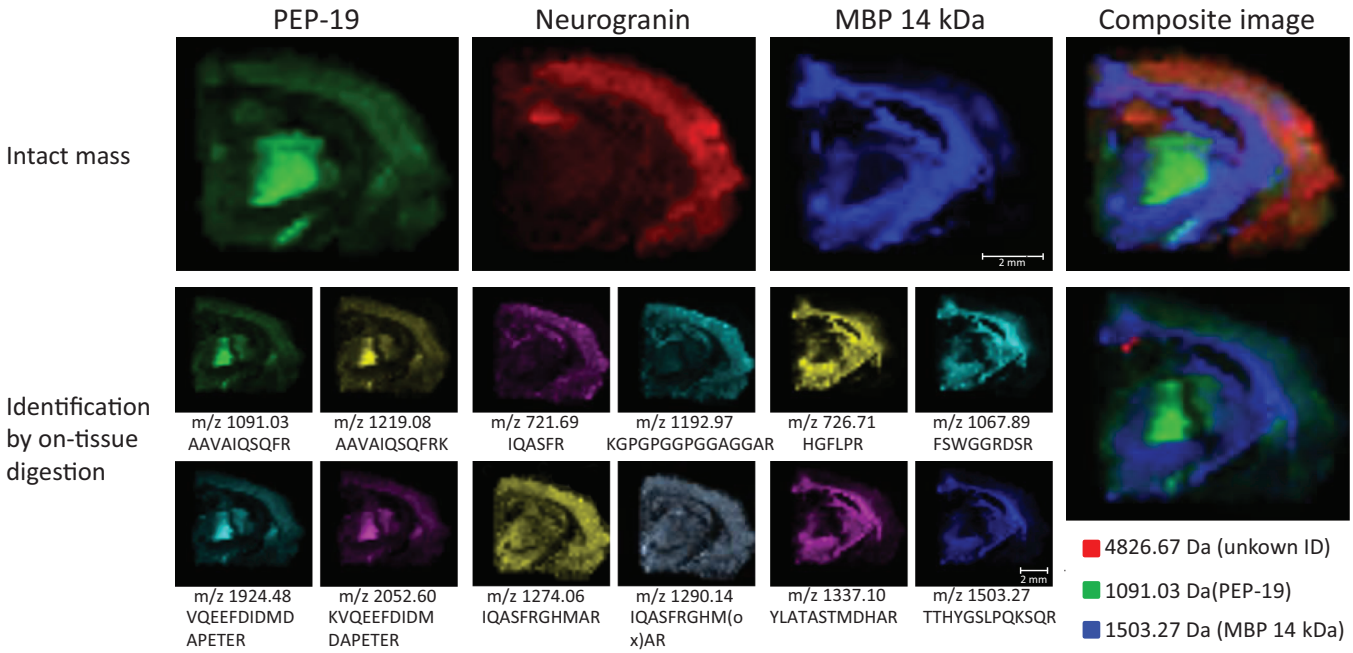

FIG. 6. On-tissue tryptic digestion MALDI IMS of hippocampus in a rat neonatally treated on PND 9–10 with BMAA (460 mg/kg). The identities of three selected proteins were validated by comparing the distribution of tryptic peptides with the distribution of the intact mass of proteins of interest (upper panel). The upper right composite image shows the localization of all three proteins. The small images (lower panels) show the tryptic peptides generated from the digestion of PEP-19, neurogranin, and MBP 14.2 kDa. The lower right composite image shows an unidentified mass 4826.67 Da in red that was uniquely detected in the area containing birefringent, granular material in the CA1 of hippocampus.

hippocampus 6 months after the neonatal exposure, whereas no histopathological changes were observed in the striatum, substantia nigra, cingulate cortex, and retrosplenial granular cortex. Intraneuronal precipitation of calcium is known to occur following excessive activation of excitatory amino acid receptors in the brain (Rodriguez *et al*., 2000), and neuronal calcification has been detected following exposure to a number of excitotoxic glutamate receptor agonists (Bernal *et al*., 2000; Gramsbergen and van den Berg, 1994; Herrmann *et al*., 1998; Petegnief *et al*., 1999; Rodriguez *et al*., 2000; Stewart *et al*., 1995). The calcium deposits may form within blebs in injured cells, or as a part of cellular membrane degradation products (Kim, 1995). BMAA is a glutamate receptor agonist that increases intracellular calcium concentrations in brain slices and cultured neuronal cells (Copani *et al*., 1991; Cucchiaroni *et al*., 2010; Lobner *et al*., 2007; Rao *et al*., 2006). Glutamate receptors have distinct regional and temporal expression profiles, often with transient peak levels during the first neonatal weeks in rats. Indeed, the number of glutamate-binding sites in the hippocampus peak at PND 9 (McDonald and Johnston, 1990). Most of the NMDA receptor subunit mRNA expression levels are at their highest during the same period (Monyer *et al*., 1994), suggesting that the high susceptibility toward BMAA during the neonatal period may be related to the peak expression of glutamate receptors. The observed mineralization of CA1 neurons in the neonatally exposed adult rats could be due to an initial activation of glutamate receptors leading to excitotoxicity. The BMAA-induced long-term neuronal degeneration and cell loss in the CA1 of hippocampus of adult animals may, however, also involve other mechanisms of toxicity such as a misincorporation of BMAA into protein which could possibly render misfolded and aggregation prone proteins to induce deleterious effects (Field *et al*., 2011).

This study also showed that the high BMAA dose elicited a markedly increased number of GFAP-immunopositive glial cells, implying astrogliosis in the CA1 segment of the rat hippocampus 6 months after the neonatal exposure. Protein analysis by MALDI IMS revealed increased levels of several histones (H2, H3, and H4) in the hippocampus which probably reflects the astrogliosis in the area, either as a consequence of proliferation or infiltration of astrocytes. In addition, MALDI IMS indicated that the levels of the astrocytic protein S100β were increased in the CA1 of hippocampus. Secreted S100β appears to stimulate glial cell proliferation and neurite outgrowth (Selinfreund *et al*., 1991). S100β may also play a role in the observed calcification of neurons in the adult hippocampus of BMAA-treated neonates, because this calcium binding protein has been shown to increase the intracellular calcium concentration by opening voltage-dependent Ca^{2+} channels and depletion of internal Ca^{2+} stores (Barger and Van Eldik, 1992; Fulle *et al*., 1997).

MALDI IMS also demonstrated that the calmodulin-regulating protein neurogranin was significantly decreased in CA1 of high-dose animals; although not statistically significant, a similar trend was observed in the low-dose group. This alteration

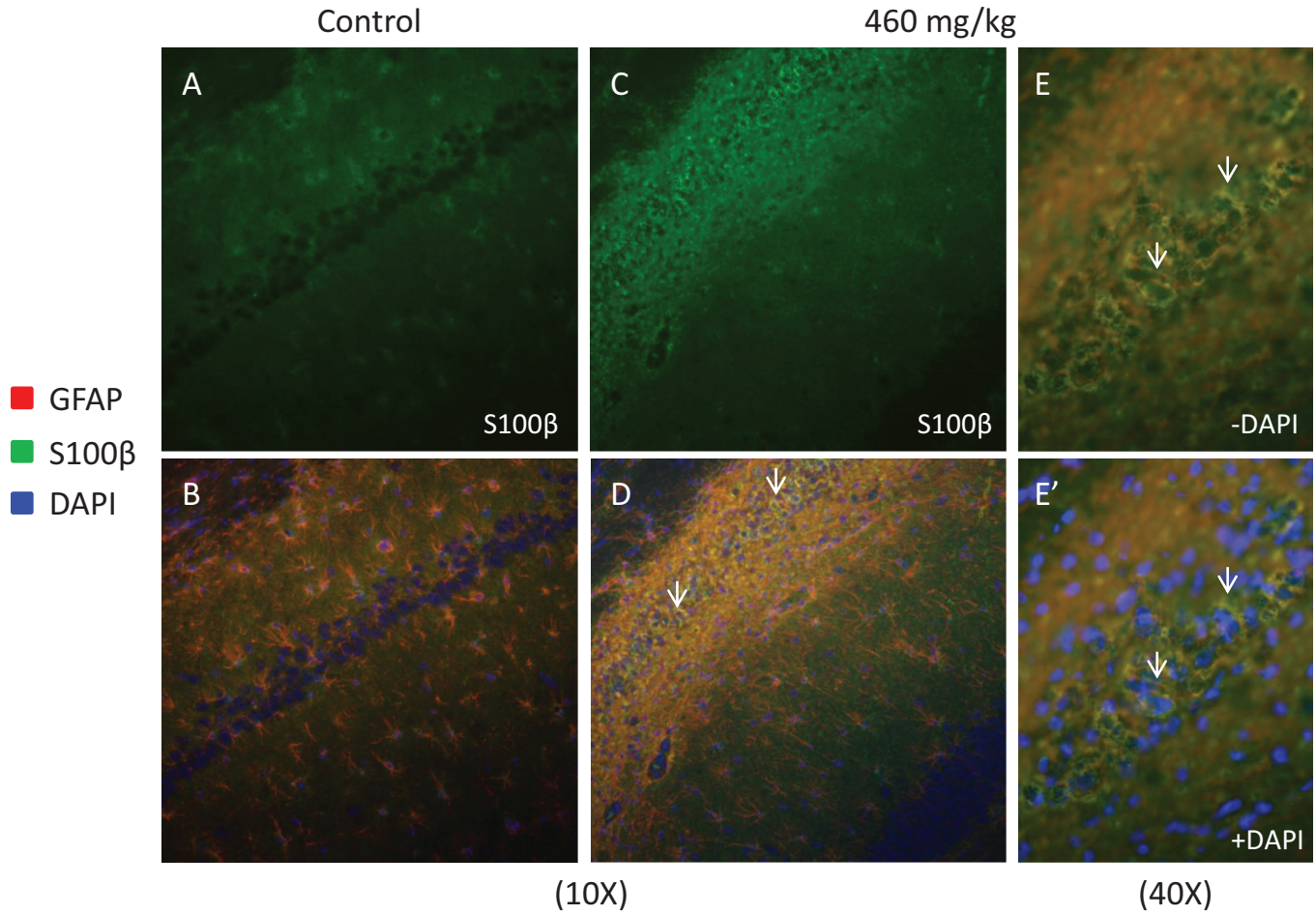

FIG. 7. Immunofluorescence showing the expression of S100β in the hippocampus (CA1 segment) of rats treated neonatally on PND 9–10 with BMAA (460 mg/kg) or vehicle. (A) Low levels of S100β immunofluorescence was detected in normal control animals. (B) Double-antigen IHC for GFAP revealed that S100β was mostly localized to the cytoplasm of astrocytes (yellow signifies overlap). (C–E') A distinct increase in immunoreactivity was seen in the CA1 segment of a BMAA-treated rat, where S100β immunofluorescence displayed typical circular forms surrounding DAPI-positive nuclei of GFAP-positive astrocytes (D, E, and E', arrows). Magnifications: A–D lens ×10; E lens ×40.

could be of importance for the observed learning and memory impairments in adult animals following neonatal exposure, because neurogranin knockout mice are reported to have severe deficits in spatial and emotional learning and a decrease in long-term potentiation induction (Diez-Guerra, 2010; Miyakawa *et al*., 2001). The similar reduction in the levels of the calcium-binding protein calmodulin and the calmodulin-binding protein BASP1/NAP22 further implicates disturbances in neuronal sprouting and plasticity (Gouraud *et al*., 2007).

Several proteins involved in neuronal transmembrane signaling displayed an about 2-fold reduced peak intensity in the animals with CA1 lesions, e.g., guanine nucleotide-binding protein gamma-7 subunit (Gng7) and Gng2. The significant decrease in the G-protein subunits suggests perturbation of G-protein-coupled receptor signaling in these animals. In contrast, the levels of several as yet unidentified proteins were significantly increased in CA1 region of these animals (e.g., 10.6 and 11.7 kDa). These protein changes could also be of importance for the development of neuronal loss and astrogliosis in the CA1 region. It cannot be excluded, however, that some of the changes in protein levels in these animals may be secondary to the decreased number of neurons in the CA1 region.

In the high-dose animals, immunohistochemical analysis revealed ubiquitin- and α-synuclein-positive staining in the CA1 region, whereas staining for tau, amyloid, and neurofilament was negative. Astrocytes were positively stained for ubiquitin, as were some of the degenerating and/or calcified neurons although not as intensely as the astrocytes. In contrast, the MALDI IMS results showed reduced levels of free ubiquitin by 60% in the affected area. Because the immunohistochemical staining was done with an antibody recognizing both free and incorporated ubiquitin, the combined data suggest the presence of highly polyubiquitinated proteins in this brain region.

The glutamatergic system is known to be involved in the modulation of many of the events that occur during the

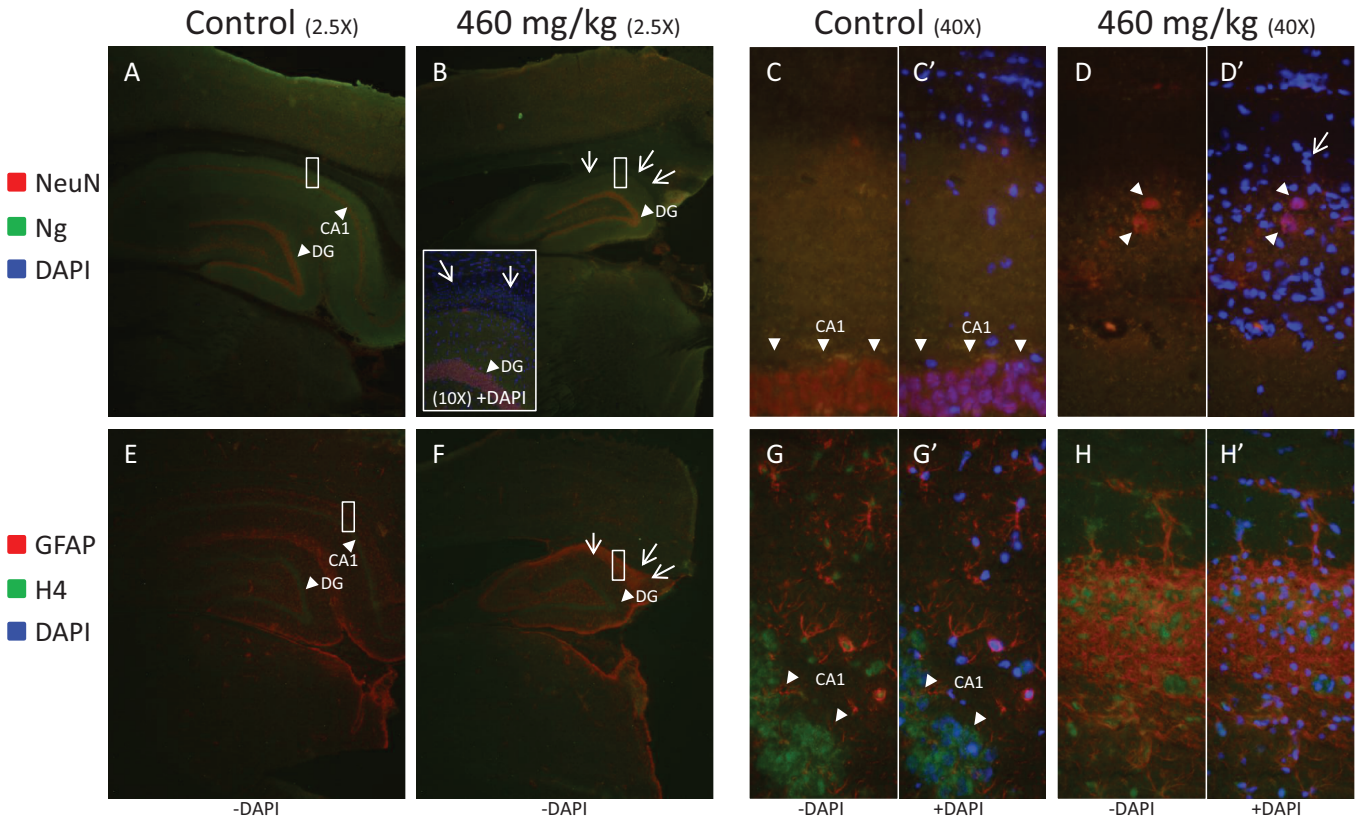

FIG. 8. Immunofluorescence of brain sections of adult rats neonatally treated on PND 9–10 with BMAA (460 mg/kg) or vehicle. (A and B) As second means of validation of MALDI IMS results, double-antigen immunofluorescence for the neuronal nuclear antigen NeuN and cytoplasmic neurogranin (Ng) confirmed loss of Ng immunoreactivity in CA1 in hippocampus of BMAA treated animals (B and insert, arrows) compared with vehicle-treated control (A). (C and D) Higher magnification of the boxed area in A and B revealed that the BMAA-induced loss of NeuN immunoreactive CA1 neurons (arrowheads) was almost complete, whereas the general nuclear staining DAPI highlighted an elevation of the number of non-neuronal cells in the same area (arrow, cf. D' and C'). (E and F) A high proportion of the non-neuronal cells were identified as astrocytes using an antibody for GFAP. (G and H) Higher magnification of the boxed area in E and F showed that both neurons and astrocytes were histone H4 immunopositive; however, BMAA appears to have caused glial scarring in CA1 and the high number of astrocytes in CA1 may account for the increase in histone H4 peak intensity seen in the MALDI IMS data. Magnifications: left part lens ×2.5; right part lens ×40.

development and neonatal exposure to BMAA could potentially disturb many processes during the development. In this study, we have shown that developmental BMAA exposure to a lower dose (150 mg/kg) induced decreased levels of proteins involved in energy metabolism and neuronal signaling in the adult hippocampus, whereas no distinct histopathological lesions were observed at this dose. Exposure to a high dose (460 mg/kg) induced changes in the expression of S100β, histones, calcium- and calmodulin-binding proteins, as well as guanine nucleotide-binding proteins. This dose also gave rise to severe lesions in the adult hippocampus including neuronal degeneration, cell loss, calcium deposits, and astrogliosis. Dietary exposure to BMAA has been suggested to contribute to neurodegenerative disease, but experimental long-term *in vivo* studies supporting this hypothesis are limited. The long-term changes in protein expressions in the hippocampus observed after a low-neonatal BMAA exposure could indicate subtle, but permanent effects of BMAA in this brain region but further studies are needed to demonstrate whether the changed protein levels are critical for neurodegeneration. Histopathological studies are also needed to explore how mineralization develops in response to exposure to BMAA. The detection of BMAA in molluscs and fish used for human consumption stresses the importance of evaluating the magnitude of human exposure to this cyanobacterial toxin (Brand *et al*., 2010; Jonasson *et al*., 2010).

SUPPLEMENTARY DATA

Supplementary data are available online at http://toxsci.oxfordjournals.org/.

FUNDING

Swedish Research Council FORMAS (E.B.B.); Swedish Research Council (522-2006-6414 to M.A., 521-2007-5407 to M.A.).

ACKNOWLEDGMENTS

Ms Raili Engdahl is gratefully acknowledged for technical assistance.

REFERENCES

Aerni, H. R., Cornett, D. S., and Caprioli, R. M. (2006). Automated acoustic matrix deposition for MALDI sample preparation. *Anal. Chem.* **78,** 827–834.

Andersson, M., Groseclose, M. R., Deutch, A. Y., and Caprioli, R. M. (2008). Imaging mass spectrometry of proteins and peptides: 3D volume reconstruction. *Nat. Methods* **5,** 101–108.

Banack, S. A., and Cox, P. A. (2003). Biomagnification of cycad neurotoxins in flying foxes: Implications for ALS-PDC in Guam. *Neurology* **61,** 387–389.

Banack, S. A., Johnson, H. E., Cheng, R., and Cox, P. A. (2007). Production of the neurotoxin BMAA by a marine cyanobacterium. *Mar. Drugs* **5,** 180–196.

Barger, S. W., and Van Eldik, L. J. (1992). S100 beta stimulates calcium fluxes in glial and neuronal cells. *J. Biol. Chem.* **267,** 9689–9694.

Bernal, F., Saura, J., Ojuel, J., and Mahy, N. (2000). Differential vulnerability of hippocampus, basal ganglia, and prefrontal cortex to long-term NMDA excitotoxicity. *Exp. Neurol.* **161,** 686–695.

Brand, L. E., Pablo, J., Compton, A., Hammerschlag, N., and Mash, D. C. (2010). Cyanobacterial blooms and the occurrence of the neurotoxin beta-N-methylamino-L-alanine (BMAA) in South Florida aquatic food webs. *Harmful Algae* **9,** 620–635.

Caller, T. A., Doolin, J. W., Haney, J. F., Murby, A. J., West, K. G., Farrar, H. E., Ball, A., Harris, B. T., and Stommel, E. W. (2009). A cluster of amyotrophic lateral sclerosis in New Hampshire: A possible role for toxic cyanobacteria blooms. *Amyotroph. Lateral Scler.* **10**(Suppl. 2), 101–108.

Caprioli, R. M., Farmer, T. B., and Gile, J. (1997). Molecular imaging of biological samples: Localization of peptides and proteins using MALDI-TOF MS. *Anal. Chem.* **69,** 4751–4760.

Copani, A., Canonico, P. L., Catania, M. V., Aronica, E., Bruno, V., Ratti, E., van Amsterdam, F. T., Gaviraghi, G., and Nicoletti, F. (1991). Interaction between beta-N-methylamino-L-alanine and excitatory amino acid receptors in brain slices and neuronal cultures. *Brain Res.* **558,** 79–86.

Cox, P. A., Banack, S. A., Murch, S. J., Rasmussen, U., Tien, G., Bidigare, R. R., Metcalf, J. S., Morrison, L. F., Codd, G. A., and Bergman, B. (2005). Diverse taxa of cyanobacteria produce beta-N-methylamino-L-alanine, a neurotoxic amino acid. *Proc. Natl. Acad. Sci. U.S.A.* **102,** 5074–5078.

Cucchiaroni, M. L., Viscomi, M. T., Bernardi, G., Molinari, M., Guatteo, E., and Mercuri, N. B. (2010). Metabotropic glutamate receptor 1 mediates the electrophysiological and toxic actions of the cycad derivative beta-N-Methylamino-L-alanine on substantia nigra pars compacta DAergic neurons. *J. Neurosci.* **30,** 5176–5188.

Diez-Guerra, F. J. (2010). Neurogranin, a link between calcium/calmodulin and protein kinase C signaling in synaptic plasticity. *IUBMB Life* **62,** 597–606.

Eriksson, P. (1997). Developmental neurotoxicity of environmental agents in the neonate. *Neurotoxicology* **18,** 719–726.

Eriksson, P., Ankarberg, E., and Fredriksson, A. (2000). Exposure to nicotine during a defined period in neonatal life induces permanent changes in brain nicotinic receptors and in behaviour of adult mice. *Brain Res.* **853,** 41–48.

Esterhuizen, M., and Downing, T. G. (2008). Beta-N-methylamino-L-alanine (BMAA) in novel South African cyanobacterial isolates. *Ecotoxicol. Environ. Saf.* **71,** 309–313.

Field, N. C., Caller, T. A., and Stommel, E. W. (2011). An explanation for the changes in collagen in sporadic amyotrophic lateral sclerosis. *Med. Hypotheses* **77,** 565–567.

Freeman, K. S. (2010). Harmful algal blooms. Musty warnings of toxicity. *Environ. Health Perspect.* **118,** A473.

Fulle, S., Mariggiò, M. A., Belia, S., Nicoletti, I., and Fanò, G. (1997). Nerve growth factor inhibits apoptosis induced by S-100 binding in neuronal PC12 cells. *Neuroscience* **76,** 159–166.

Gouraud, S. S., Heesom, K., Yao, S. T., Qiu, J., Paton, J. F., and Murphy, D. (2007). Dehydration-induced proteome changes in the rat hypothalamo-neurohypophyseal system. *Endocrinology* **148,** 3041–3052.

Gramsbergen, J. B., and van den Berg, K. J. (1994). Regional and temporal profiles of calcium accumulation and glial fibrillary acidic protein levels in rat brain after systemic injection of kainic acid. *Brain Res.* **667,** 216–228.

Groseclose, M. R., Andersson, M., Hardesty, W. M., and Caprioli, R. M. (2007). Identification of proteins directly from tissue: In situ tryptic digestions coupled with imaging mass spectrometry. *J. Mass Spectrom.* **42,** 254–262.

Hanrieder, J., Ljungdahl, A., and Andersson, M. (2012). MALDI imaging mass spectrometry of neuropeptides in Parkinson's disease. *J. Vis. Exp.* **60,** 3445.

Hanrieder, J., Wicher, G., Bergquist, J., Andersson, M., and Fex-Svenningsen, A. (2011). MALDI mass spectrometry based molecular phenotyping of CNS glial cells for prediction in mammalian brain tissue. *Anal. Bioanal. Chem.* **401,** 135–147.

Herrmann, G., Stünitz, H., and Nitsch, C. (1998). Composition of ibotenic acid-induced calcifications in rat substantia nigra. *Brain Res.* **786,** 205–214.

Helle, K. B. (2010). Regulatory peptides from chromogranin A and secretogranin II. *Cell. Mol. Neurobiol.* **30,** 1145–1146.

Janus, C., and Welzl, H. (2010). Mouse models of neurodegenerative diseases: Criteria and general methodology. *Methods Mol. Biol.* **602,** 323–345.

Jonasson, S., Eriksson, J., Berntzon, L., Spácil, Z., Ilag, L. L., Ronnevi, L. O., Rasmussen, U., and Bergman, B. (2010). Transfer of a cyanobacterial neurotoxin within a temperate aquatic ecosystem suggests pathways for human exposure. *Proc. Natl. Acad. Sci. U.S.A.* **107,** 9252–9257.

Karamyan, V. T., and Speth, R. C. (2008). Animal models of BMAA neurotoxicity: A critical review. *Life Sci.* **82,** 233–246.

Karlsson, O., Berg, C., Brittebo, E. B., and Lindquist, N. G. (2009a). Retention of the cyanobacterial neurotoxin beta-N-methylamino-l-alanine in melanin and neuromelanin-containing cells–a possible link between Parkinson-dementia complex and pigmentary retinopathy. *Pigment Cell Melanoma Res.* **22,** 120–130.

Karlsson, O., Lindquist, N. G., Brittebo, E. B., and Roman, E. (2009b). Selective brain uptake and behavioral effects of the cyanobacterial toxin BMAA (beta-N-methylamino-L-alanine) following neonatal administration to rodents. *Toxicol. Sci.* **109,** 286–295.

Karlsson, O., Roman, E., Berg, A. L., and Brittebo, E. B. (2011). Early hippocampal cell death, and late learning and memory deficits in rats exposed to the environmental toxin BMAA (beta-N-methylamino-L-alanine) during the neonatal period. *Behav. Brain Res.* **219,** 310–320.

Karlsson, O., Roman, E., and Brittebo, E. B. (2009c). Long-term cognitive impairments in adult rats treated neonatally with beta-N-methylamino-L-Alanine. *Toxicol. Sci.* **112,** 185–195.

Kim, K. M. (1995). Apoptosis and calcification. *Scanning Microsc.* **9,** 1137–75; discussion 1175.

Ljungdahl, A., Hanrieder, J., Fälth, M., Bergquist, J., and Andersson, M. (2011). Imaging mass spectrometry reveals elevated nigral levels of dynorphin neuropeptides in L-DOPA-induced dyskinesia in rat model of Parkinson's disease. *PLoS ONE* **6,** e25653.

Lobner, D., Piana, P. M., Salous, A. K., and Peoples, R. W. (2007). Beta-N-methylamino-L-alanine enhances neurotoxicity through multiple mechanisms. *Neurobiol. Dis.* **25,** 360–366.

Mathur, B. N., Caprioli, R. M., and Deutch, A. Y. (2009). Proteomic analysis illuminates a novel structural definition of the claustrum and insula. *Cereb. Cortex* **19,** 2372–2379.

McDonald, J. W., and Johnston, M. V. (1990). Physiological and pathophysiological roles of excitatory amino acids during central nervous system development. *Brain Res. Brain Res. Rev.* **15,** 41–70.

Metcalf, J. S., Banack, S. A., Lindsay, J., Morrison, L. F., Cox, P. A., and Codd, G. A. (2008). Co-occurrence of beta-N-methylamino-L-alanine, a neurotoxic amino acid with other cyanobacterial toxins in British waterbodies, 1990-2004. *Environ. Microbiol.* **10,** 702–708.

Miyakawa, T., Yared, E., Pak, J. H., Huang, F. L., Huang, K. P., and Crawley, J. N. (2001). Neurogranin null mutant mice display performance deficits on spatial learning tasks with anxiety related components. *Hippocampus* **11,** 763–775.

Montine, T. J., Li, K., Perl, D. P., and Galasko, D. (2005). Lack of beta-methylamino-l-alanine in brain from controls, AD, or Chamorros with PDC. *Neurology* **65,** 768–769.

Monyer, H., Burnashev, N., Laurie, D. J., Sakmann, B., and Seeburg, P. H. (1994). Developmental and regional expression in the rat brain and functional properties of four NMDA receptors. *Neuron* **12,** 529–540.

Murch, S. J., Cox, P. A., Banack, S. A., Steele, J. C., and Sacks, O. W. (2004). Occurrence of beta-methylamino-l-alanine (BMAA) in ALS/PDC patients from Guam. *Acta Neurol. Scand.* **110,** 267–269.

Pablo, J., Banack, S. A., Cox, P. A., Johnson, T. E., Papapetropoulos, S., Bradley, W. G., Buck, A., and Mash, D. C. (2009). Cyanobacterial neurotoxin BMAA in ALS and Alzheimer's disease. *Acta Neurol. Scand.* **120,** 216–225.

Paxinos, G., and Watson, C. (2007). *The Rat Brain in Stereotaxic Coordinates*, 6th ed. Academic Press, Oxford, U.K.

Perry, T. L., Bergeron, C., Biro, A. J., and Hansen, S. (1989). Beta-N-methylamino-L-alanine. Chronic oral administration is not neurotoxic to mice. *J. Neurol. Sci.* **94,** 173–180.

Petegnief, V., Saura, J., Dewar, D., Cummins, D. J., Dragunow, M., and Mahy, N. (1999). Long-term effects of alpha-amino-3-hydroxy-5-methyl-4-isoxazole propionate and 6-nitro-7-sulphamoylbenzo(f)quinoxaline-2,3-dione in the rat basal ganglia: Calcification, changes in glutamate receptors and glial reactions. *Neuroscience* **94,** 105–115.

Pierson, J., Norris, J. L., Aerni, H. R., Svenningsson, P., Caprioli, R. M., and Andrén, P. E. (2004). Molecular profiling of experimental Parkinson's disease: Direct analysis of peptides and proteins on brain tissue sections by MALDI mass spectrometry. *J. Proteome Res.* **3,** 289–295.

Rao, S. D., Banack, S. A., Cox, P. A., and Weiss, J. H. (2006). BMAA selectively injures motor neurons via AMPA/kainate receptor activation. *Exp. Neurol.* **201,** 244–252.

Rodriguez, M. J., Bernal, F., Andrés, N., Malpesa, Y., and Mahy, N. (2000). Excitatory amino acids and neurodegeneration: A hypothetical role of calcium precipitation. *Int. J. Dev. Neurosci.* **18,** 299–307.

Selinfreund, R. H., Barger, S. W., Pledger, W. J., and Van Eldik, L. J. (1991). Neurotrophic protein S100 beta stimulates glial cell proliferation. *Proc. Natl. Acad. Sci. U.S.A.* **88,** 3554–3558.

Skold, K., Svensson, M., Nilsson, A., Zhang, X., Nydahl, K., Caprioli, R. M., Svenningsson, P., and Andrén, P. E. (2006). Decreased striatal levels of PEP-19 following MPTP lesion in the mouse. *J. Proteome Res.* **5,** 262–269.

Smith, Q. R., Nagura, H., Takada, Y., and Duncan, M. W. (1992). Facilitated transport of the neurotoxin, beta-N-methylamino-L-alanine, across the blood-brain barrier. *J. Neurochem.* **58,** 1330–1337.

Snyder, L. R., Cruz-Aguado, R., Sadilek, M., Galasko, D., Shaw, C. A., and Montine, T. J. (2009). Lack of cerebral BMAA in human cerebral cortex. *Neurology* **72,** 1360–1361.

Spencer, P. S., Nunn, P. B., Hugon, J., Ludolph, A. C., Ross, S. M., Roy, D. N., and Robertson, R. C. (1987). Guam amyotrophic lateral sclerosis-Parkinsonism-dementia linked to a plant excitant neurotoxin. *Science* **237,** 517–522.

Steele, J. C., and McGeer, P. L. (2008). The ALS/PDC syndrome of Guam and the cycad hypothesis. *Neurology* **70,** 1984–1990.

Stewart, G. R., Olney, J. W., Schmidt, R. E., and Wozniak, D. F. (1995). Mineralization of the globus pallidus following excitotoxic lesions of the basal forebrain. *Brain Res.* **695,** 81–87.

Valerio, E., Chaves, S., and Tenreiro, R. (2010). Diversity and impact of prokaryotic toxins on aquatic environments: A review. *Toxins (Basel).* **2,** 2359–2410.

Wong-Riley, M. T. (1989). Cytochrome oxidase: An endogenous metabolic marker for neuronal activity. *Trends Neurosci.* **12,** 94–101.